Submitted to Journal of Engineering Materials and Technology, December 2018

The Precise Determination of the Johnson-Cook Material and Damage Model Parameters and Mechanical Properties of Aluminum 7068-T651 Alloy

B. Bal[1,*], K. K. Karaveli[1], B. Cetin[2], B. Gumus[3]

[1] Department of Mechanical Engineering, Abdullah Gül University, 38080 Kayseri, Turkey

[2] FNSS Defense Systems Co. Inc., 06830, Golbasi, Ankara, Turkey

[3] ASELSAN A.Ş. 06370 Ankara, Turkey

Abstract

Al 7068-T651 alloy is one of the recently developed materials used mostly in the defense industry due to its high strength, toughness and low weight compared steels. The aim of this study is to identify the Johnson-Cook (J-C) material model parameters, the accurate Johnson-Cook (J-C) damage parameters, D_1, D_2 and D_3 of the Al 7068-T651 alloy for Finite Elemental Analysis (FEA) based simulation techniques, together with other damage parameters, D_4 and D_5. In order to determine D_1, D_2 and D_3 tensile tests were conducted on notched and smooth specimens at medium strain rate, 10^0 s^{-1}, and tests were repeated 7 times to ensure the consistency of the results both in the rolling direction and perpendicular to the rolling direction. To determine D_4 and D_5, further tensile tests were conducted on specimens at high strain rate (10^2 s^{-1}) and temperature (300 °C) by means of Gleeble Thermal-mechanical Physical Simulation system. The final areas of fractured specimens were calculated through optical microscopy. The effects of stress triaxiality factor, rolling direction, strain rate and temperature on the mechanical properties of Al 7068-T651 alloy were also investigated. Damage parameters were calculated via Levenberg-Marquardt optimization method. From all the aforementioned experimental work, J-C material model parameters were

[*]Corresponding author. burak.bal@agu.edu.tr.

also determined. In this article, J-C damage model constants, based on maximum and minimum equivalent strain values, were also reported which can be utilized for the simulation of different applications.

Keywords: Aluminum, Johnson-Cook material model, Johnson-Cook damage model rolling direction, Mechanical Testing.

1. Introduction

High strength and lightweight materials have become the materials of choice for several applications [1]. Among other metallic materials, aluminum (Al) alloys, which have face-centered cubic (FCC) crystal structure at room temperature, are one of the most popular materials due to their promising mechanical properties [2,3]. Aluminum 7000 series has been widely used in automobile, machinery, aerospace and defense industries due to its excellent combinations of low weight, high strength, good machinability and high corrosion resistance [4,5]. Al 7068-T651 alloy is the strongest aluminum commercially produced with 6-8% zinc as a predominant element in its chemical composition [6]. In the mid 1990's, this alloy was developed by Kaiser Aluminum and designed as an alternative to Al 7075 alloys for applications which require greater strength at both room and elevated temperatures. In particular, compared to Al 7075 alloy, it has similar corrosion resistance, promising ductility and 30% higher yield strength [6,7]. Thus, Al 7068-T651 alloy, which has greater strength and lower weight than Al 7075, is a better material of choice for several industries, such as automotive, aviation and defense. Therefore, the precise determination of the mechanical response of Al 7068-T651 alloy under several loading scenarios and the development of a constitutive material and damage models are of great importance to increase the accuracy of finite element analyses (FEA) and to utilize this material on the aforementioned applications.

Journal of Engineering Materials and Technology. Received December 26, 2018;
Accepted manuscript posted February 06, 2019. doi:10.1115/1.4042870

Different plasticity and failure models have been developed to describe the flow stress and deformation behavior of materials under various conditions in finite element modeling (FEM) for various applications [8–11]. Among others, Johnson-Cook (J-C), which includes strain hardening, strain rate hardening and thermal softening, is the most widely used material model [12]. Therefore, the precise determination of J-C material model and damage parameters is of utmost importance to obtain the realistic FEM results. J-C material and damage parameters are generally obtained by the material response under tensile and Split-Hopkinson loading scenarios [13]. Due to the nature of materials, several factors affect this material response, such as rolling direction, temperature and strain rate. In the current literature, the effects of temperature and strain rate have been well-studied but the effect of rolling direction on J-C damage parameters have not been investigated in detail [14]. In addition, even though there are high number of studies on determination of J-C material model and damage parameters of Al alloys [15–18], the reported results are different from one another due to several reasons. First, the number of experimental repetitions used in these studies to ensure the consistency of material response is not enough to determine precise J-C damage parameters. Second, the J-C damage parameters are determined by considering only the average equivalent failure strain. Consequently, to the best of the authors' knowledge, there is no study which determines the Johnson-Cook damage model parameters of Al 7068-T651 considering different rolling directions and anisotropy, with a high number of experimental repetitions, and aiming different applications. Therefore, the aim of this study can be summarized as: 1) To determine the mechanical response of Al 7068-T651 under different loading conditions, 2) To obtain precise J-C damage model parameters of Al 7068-T651 along different rolling directions, 3) To propose different J-C damage parameters for different applications, 4) To obtain J-C material model parameters of Al 7068-T651.

Journal of Engineering Materials and Technology. Received December 26, 2018;
Accepted manuscript posted February 06, 2019. doi:10.1115/1.4042870

In this study, the mechanical behavior of Al 7068-T651 was determined by tensile, Split-Hopkinson Pressure Bar (SHPB) and Gleeble tests in order to meet the objectives listed above and fill the gap in the literature. Firstly, tensile tests at medium strain rate, i.e. 10^0 s^{-1}, were conducted 7 times to ensure the consistency of results. Samples were taken from materials both in the rolling direction and perpendicular to the rolling direction to determine the J-C damage parameters, (D_1, D_2 and D_3), of Al 7068-T651 alloy precisely. Therefore, both the effects of rolling direction and stress concentration, induced by notch on the sample surface to produce localized plasticity, on the overall material response of the Al 7068-T651 alloy were determined. Moreover, using maximum, average and minimum equivalent failure strain values, different J-C damage parameters were determined for several applications. In addition, Gleeble and SHPB tests were conducted at different strain rates and temperatures in order to obtain the mechanical response precisely under different loading conditions and determine the J-C material model and the rest of the J-C damage parameters. Since the precision of Gleeble and SHPB tests are reasonably high, these tests were conducted 3 times. In order to solve an overdetermined system and to obtain J-C damage parameters for different application areas, an iterative Levenberg-Marquardt least squares method [19,20] was used. In particular, the methodology of the Levenberg-Marquardt least squares method was transferred to the Matlab environment. Overall, the work presented herein exhibits the precise J-C damage parameters, which can be used for accurate damage simulations in FEA for different application areas of Al 7068-T651 alloy, as well as the J-C material model parameters and the effects of rolling direction and notch radius on the material response of Al 7068-T651 alloy. Consequently, this study constitutes an important guideline for the selection and usage of the aforementioned parameters in Finite Element simulations.

2. Experimental Procedures and Results

Aluminum 7068-T651 alloy is the investigated material in the current study. The chemical composition of the studied material is illustrated in Table 1. The chemical composition has been studied by Energy-Dispersive X-ray (EDX) spectroscopy. In order to produce this material, solution heat treatment process was applied to Al 7068-T651 alloy, which is then stress relieved by stretching and then artificially aged. By turning and milling operations, test specimens were prepared and then polished to get rid of all flaws and residual stresses on the material's surface. The samples were prepared in two groups: along the rolling direction and perpendicular to the rolling direction. Specimens perpendicular to the rolling direction were only tested under uniaxial tensile loading to determine the effects of rolling direction on J-C damage parameters, D_1, D_2, D_3.

In order to determine the effects of stress triaxiality, corresponding mechanical behavior and J-C damage parameters, which were D_1, D_2 and D_3, samples were subjected to tensile loading at room temperature. J-C damage parameters were calculated using stress and strain data of specimens whose technical drawings are shown in Figure 1a, where R represents the notch radius of the notched specimens. There were four different specimen types: a smooth one and 3 notched specimens with different notch radii. Designing different specimens introduces different stress triaxiality factors (STF), σ^*, which are listed in Table 2. A servohydraulic tensile/fatigue test machine, Instron 8801, was utilized to conduct tensile tests at a strain rate of 10^0 s^{-1} and at room temperature.

To ensure the accuracy of results, seven identical samples were tested. In total, 56 tensile tests were performed, consisting of eight sample types and seven repetitions. Displacement and force data were measured by the extensometer and load cell of the servohydraulic tensile/fatigue test machine, respectively. By using classical elasticity-

plasticity equations, both engineering and true stress and strain values of specimens were obtained [21].

After the tensile tests, the diameters of the ellipsoidal fractured cross sectional areas of the specimens were measured by an optical microscope, EUROMEX NexiusZoom. The corresponding cross sectional areas were then calculated from the classical ellipse equation that is defined as:

$$x^2/a^2 + y^2/b^2 = 1 \quad (1)$$

where x and y are the coordinates of a point on the ellipse, and a and b are the radii on the x and y coordinates, respectively.

For the determination of the J-C material model parameters and the rest of J-C damage model parameters, Gleeble and SHPB tests were also conducted. Gleeble 3800-GTC system was utilized for Gleeble tests and a custom made experimental setup (Figure 2) was used for SHPB tests. Technical drawings of the Gleeble and SHPB samples are shown in Figure 1b and Figure 1c, respectively. Gleeble tests were conducted at two different strain rates, 0.001 and 10^2 s^{-1}, and two different temperatures, room temperature (25 °C) and 300 °C. In addition, compression type SHPB tests were conducted at an initial strain rates of 1800, 2500 and 5000 s^{-1} at RT. Gleeble and SHPB tests were repeated 3 times to ensure the accuracy of results and the standard deviation in the results showed that these tests were very precise.

3. Theory and Calculations

3.1 Johnson-Cook constitutive model

The empirical J-C model is practical for describing the stress and strain relations of metals under conditions of large deformation, high strain rate and high temperature [22]. By

using limited data from experiments, J-C model well predicts the mechanical properties of metals. The general expression can be defined as:

$$\sigma = [A + B\varepsilon^n][1 + CLn(\dot{\varepsilon}^*)][1 - T^{*m}] \quad (2)$$

where σ is the equivalent flow stress, A is the yield stress of the material under reference deformation conditions (unit is MPa), B is the strain hardening constant (unit is MPa), C is the strain rate strengthening coefficient, n is the strain hardening coefficient, m is the temperature softening of the material through homologous temperature, T^*, $\dot{\varepsilon}^*$ is the dimensionless strain rate $[\dot{\varepsilon}^* = \dot{\varepsilon}/\dot{\varepsilon}_0]$ where $\dot{\varepsilon}$ is the equivalent plastic strain, and $\dot{\varepsilon}_0$ is the reference strain rate. T^* can be calculated through $T^* = (T - T_{ref})/(T_m - T_{ref})$ where T_m is the melting temperature of the material and T_{ref} is the reference deformation temperature. In equation 2, $[A + B\varepsilon^n]$ and $[1 + CLn(\dot{\varepsilon}^*)]$ represent the strain hardening effect and strain rate effect, respectively, while $[1 - T^{*m}]$ stands for the temperature softening effect. The aforementioned J-C model parameters were calculated by using the results of SHPB and Gleeble tests.

3.2 Johnson-Cook failure model

The J-C fracture criterion makes the failure strain sensitive to stress triaxiality, temperature, strain rate and strain path. This model interests in damage accumulation via damage parameter. D, in equation 3, is damage variable, [0, 1]. When D is equal to 0, the material is not damaged, when it is equal to 1, the material is fully damaged. D can be defined as:

$$D = \sum_{t=0} \Delta\varepsilon_{pl}/\dot{\varepsilon} \quad (3)$$

where $\Delta\varepsilon_{pl}$ is the variation of the equivalent plastic strain.

Journal of Engineering Materials and Technology. Received December 26, 2018;
Accepted manuscript posted February 06, 2019. doi:10.1115/1.4042870

According to the J-C ductile failure model, the equivalent plastic strain for damage initiation, $\bar{\varepsilon}_f^{pl}$, depends on stress triaxiality, strain rate and temperature and it can be defined as:

$$\bar{\varepsilon}_f^{pl}(\sigma^*, \dot{\varepsilon}^{pl}, T^*) = \left[D_1 + D_2 e^{D_3 \sigma^*}\right]\left[1 + D_4 Ln\left(\dot{\varepsilon}/(\varepsilon_0)^{\cdot}\right)\right][1 + D_5 T^*] \quad (4)$$

where D_1, D_2, D_3, D_4 and D_5 are J-C damage parameters. These parameters can be calculated from the mechanical testing results. The expression in the first set of brackets represents the effect of STF. The second and the third brackets represent, respectively, strain rate effect and temperature effect. In this study, constants D_1, D_2 and D_3 were determined by performing tensile test at medium strain rate, 10^0 s^{-1}, on notched specimens (notch radii, 0.4 mm, 0.8 mm, and 2.0 mm) and smooth specimens at room temperature and D_4 and D_5 were calculated based on SHPB and Gleeble test results. STF is the ratio of hydrostatic stress to equivalent stress and is found in the range of $-\infty$ to $+\infty$. It can be expressed as:

$$STF = [\sigma_h/\sigma] \quad (5)$$

where σ_h is hydrostatic stress and σ is equivalent stress, which proves that the J-C failure model depends on the STF. On the other hand, a newer factor is used in the failure analysis of ductile metals, which is called the Lode angle or the Lode parameter (θ_L). This parameter or angle is the third invariant of deviatoric stress tensor [23].

The characteristic values of STF are 1/3 for uniaxial tensile stress (σ, 0, 0) with $\sigma > 0$, and -1/3 under uniaxial compression (σ, 0, 0) with $\sigma < 0$ for a smooth material [24]. Since notched specimens have more local deformation, STF changes and can be expressed as:

$$\sigma^* = 1/3 + Ln(1 + a_0/(2R_0)) \quad (6)$$

where a_0 is the specimen radius at the notch center and R_0 is the original specimen radius. Eq. (6) is firstly proposed by P.W. Bridgman for the case of round and notched specimens [25]. STF values for each specimen are listed in Table 2. This formulation uses a perfectly-plastic material behavior assumption which discards the strain hardening phenomena. For this reason, there is some scientific efforts to provide any possible corrections to Bridgman's formula by means of FEA simulations [26,27]. Furthermore, fracture strain formulations which takes into account the lode angle dependence are also valid in the literature [28,29]. However, at present study, the Brigdmans's formulation was used. The FEA based corrections in the ductile damage surface of Al 7068-T651 alloy and the investigation of the lode angle dependence are intended to be treated as a future wok study and not the scope of current study.

In order to determine J-C failure model constants, the equivalent plastic strain at failure, $\bar{\varepsilon}_f^{pl}$ is calculated by the Equation 7, where A_0 and A_f are the initial and final cross-section areas, respectively. After tensile test, the final cross sections of specimens are assumed to be elliptic and their diameters, which are perpendicular to each other, are measured with an optical microscope. Final cross-section areas of the specimens were calculated from the classical area of an ellipse equation. The calculated initial and final cross-section areas of the specimens are given in Table 3 for the determination of D_1, D_2 and D_3 and Table 4 for D_4 and D_5.

$$\bar{\varepsilon}_f^{pl} = Ln\, A_0/A_f \tag{7}$$

To calculate first three J-C damage parameters by using the results of uniaxial tensile tests, strain rate and temperature were assumed as stationary, therefore equation 4 can be expressed as

$$\bar{\varepsilon}_f^{pl}(\sigma^*, \dot{\bar{\varepsilon}}^{pl}, T^*) = \left[D_1 + D_2 e^{D_3 \sigma^*}\right] \quad (8)$$

Uniaxial tensile tests were conducted on 4 different specimen geometries, one of them is smooth and others are notched, which results in 4 equations for both materials in the rolling direction and perpendicular to the rolling direction. In equation 8, there are 3 unknowns, D_1, D_2 and D_3. Therefore, to solve the overdetermined system the Levenberg-Marquardt optimization method was utilized and J-C damage parameters were calculated. The optimization code was prepared in Matlab. It should be noted that, specimens perpendicular to the rolling direction were only used for the purpose of determining the effects of rolling direction on the first three J-C damage parameters.

To calculate J-C damage parameter, D_4, stress triaxiality and temperature were assumed as stationary, therefore equation 4 can be expressed as

$$\bar{\varepsilon}_f^{pl}(\sigma^*, \dot{\bar{\varepsilon}}^{pl}, T^*) = \left[1 + D_4 Ln\left(\frac{\dot{\varepsilon}}{\dot{\varepsilon}_0}\right)\right] \quad (9)$$

To calculate Johnson-Cook damage parameter, D_5, stress triaxiality and strain rate are assumed as stationary, therefore equation 4 can be expressed as

$$\bar{\varepsilon}_f^{pl}(\sigma^*, \dot{\bar{\varepsilon}}^{pl}, T^*) = [1 + D_5 T^*] \quad (10)$$

From the data obtained through Gleeble tests conducted at high strain rate (100 s^{-1}) and high temperature (300 °C) D_4 and D_5 were calculated.

In this study, D_1, D_2 and D_3 parameters were calculated based on maximum, average and minimum equivalent plastic strain values to propose different parameters for different design purposes. In addition, these parameters were determined for both rolling directions. The rest of the J-C damage and constitutive model parameters were determined based on only

the average equivalent plastic strain values and only for the specimens along the rolling direction.

4. Results and Discussion

4.1 Tensile Test Results

The mechanical responses of notched and smooth Al 7068-T651 alloy along the rolling direction and perpendicular to the rolling direction at room temperature and at medium strain rate, 10^0 s^{-1}, are illustrated in Figure 3, and the corresponding mechanical properties are listed in Table 5. The force displacement and true stress-true strain graphs of both along and perpendicular to rolling direction specimens are given in Figure 3(a-d). It is clear that the mechanical properties of the Al 7068-T651 alloy depend on both the rolling direction and notch radius, which alters STF. Specifically, the specimen along the rolling direction with a 0.4 mm notch radius, which has the highest STF, shows the best, and the smooth specimen shows the worst ductility and strength combination. On the contrary, the smooth specimen has higher strength values at the same strain values in the elastic range compared to other specimens, even though it shows less ductility than others. Also, smooth specimen shows more plasticity than notched specimens (Figure 3c). This result can be attributed to the fact that notched specimens spend the given energy to the localized deformation around the notched region elastically but cannot accommodate the given energy plastically. On the contrary, the deformation is uniform for the smooth specimens and the energy can be accommodated plastically for a certain period of time prior to the failure. Furthermore, as the STF increases, both ductility and strength values of Al 7068-T651 alloy along the rolling direction also increase. The ductility of the material increased from 0.1 to 0.5 and strength of the material increased from 819 to 1510 MPa with increasing STF. When compared to the Al

7075 alloy, these results show that Al 7068-T651 alloy along the rolling direction shows a better strength and ductility combination [15].

Figure 3b and Figure 3d show the force-displacement curves and true stress-true strain curves of Al 7068-T651 alloy perpendicular to the rolling direction at room temperature and a strain rate of 10^0 s^{-1}, respectively. It can be observed that the specimen with a 0.8 mm notch radius has a higher strength value than other specimens. However, the specimen with a 0.4 mm notch radius has the best ductility. In contrast to the rolling direction case, the specimen with a 0.4 mm notch radius has the lowest strength value and the specimen with a 2 mm notch radius has the lowest ductility. Similar to the rolling direction case, as the STF increases, ductility of the specimens that are perpendicular to the rolling direction also increases from 0.05 to 0.19. When compared to the Al 7075 alloy along the rolling direction, these results show that Al 7068-T651 alloy perpendicular to the rolling direction shows weaker mechanical strength and ductility [30].

Figure 4 shows the effect of the rolling direction on the mechanical response of Al 7068-T651 alloy. It is obvious that the mechanical properties of the Al 7068-T651 alloy are dramatically deteriorated when the rolling direction of the specimen is changed from along the rolling direction to perpendicular to the rolling direction. In particular, when the direction is changed, mechanical strength and ductility values drop by at least 21.6 % and 44.3 %, respectively. On the contrary, within the elastic range, Al 7068-T651 alloy perpendicular to the rolling direction has greater strength values at the same strain compared to materials along the rolling direction. However, they are brittle and sudden failure occurs before yield point. Therefore, Al 7068-T651 alloy in the direction perpendicular to the rolling direction can be safely used over Al 7068-T651 alloy along the rolling direction for applications that do not require high stress values. The current finding proves that Al 7068-T651 material has

anisotropic properties and the determination of these is very crucial for engineering design of this material.

The relationship between STF and equivalent failure strain for specimen along and perpendicular to the rolling direction are given in Figure 5 and Figure 6, respectively. STF and equivalent plastic strain at fracture values were calculated by using equations 6 and 7, respectively. For all specimens in both directions, the equivalent plastic strain at fracture was generally inversely proportional to STF. This behavior is expected since it is well know that as the STF increases, the structural degradation occurs earlier under tensile loading and corresponds well with previous studies [18,31]. Yet, this behavior depends on the material and the rolling direction as shown in Figure 6. The change in STF from 0.33 to 0.65 caused a slight increase in the equivalent plastic strain at fracture for the material perpendicular to the rolling direction. This behavior shows that a critical notch radius might enhance the failure strain of the Al 7068-T651 alloy perpendicular to the rolling direction. It should be noted that measuring the fracture areas by an optical microscope is not the best way to determine the equivalent plastic strain to. Instead, digital image correlation (DIC) based strain measurement techniques would give better results. Therefore, the overshooting specific to R0.8 in Figure 5 and R2 in Figure 6 can be avoided by using more advanced strain measurement techniques such as, DIC.

J-C damage model constants, D_1, D_2 and D_3 of the Al 7068-T651 alloy were computed by equation 8 using Levenberg-Marquardt optimization method. Specifically, a Matlab script was prepared to solve the overdetermined system. By using maximum, average and minimum values of the equivalent plastic strain at fracture, which are shown as red dots in Figure 5 and Figure 6, three different J-C damage constants for different application areas were computed. The computed J-C damage parameters are listed in Table 6, Table 7 and Table 8. In the

current literature, the J-C damage constant for different materials are generally calculated based on average failure strain and given as an average J-C damage parameters [32]. However, the average J-C damage parameters should be used to simulate the mechanical responses of different applications, where the reliability is not the main concern. For instance, for a car design, average J-C damage parameters (Table 7) can be used in FE simulations since both cost and safety are significant for automobile industry.

In this article, in addition to J-C damage parameters, which were calculated based on average equivalent strain values, J-C damage model constants based on maximum and minimum equivalent strain values were also determined since these can be used for the simulation of different application areas. Table 6 lists the J-C damage model constants for Al 7068-T651 alloy based on maximum equivalent plastic strain values. When safety is not the main concern for a design, these J-C damage constants (in Table 6) can be used in FE simulations, such as demanding applications. For instance, the maintenance period for race cars is very frequent and the main concern on the design of race cars is to manufacture the most lightweight and compact race car so the J-C damage parameters listed in the Table 6 can be used for the FE simulations of these kinds of application areas. On the other hand, if the material will be used applications where safety is the primary concern, such as elevators, the J-C damage model constants based on minimum equivalent plastic strain values (Table 8) can be utilized. Thus, this article opens a new venue for the usage of Al 7068-T651 alloy for different application areas. Consequently, this study is one of the first studies which precisely determine the J-C damage parameters of Al 7068-T651 alloy both along the rolling direction and perpendicular to the rolling direction for different application areas.

4.2 Split Hopkinson Pressure Bar (SHPB) Test Results

Figure 7 shows the mechanical behavior of Al 7068-T651 alloy under SHPB loading. The results are the average results of 3 different SHPB tests at 3 different strain rates. It can be clearly seen from the figure that both the elastic and plastic response of Al 7068-T651 alloy were not affected by strain rate considerably. However, it should be also noted that, there was no change in the order of magnitude of strain rates. The SHPB test results were used to determine J-C material model parameters.

4.3 Gleeble Test Results

Figure 8 shows the effects of temperature and strain rate on the true stress – true strain response of Al 7068 alloy. All the Gleeble tests were conducted three times to ensure consistency of the results. In particular, at the same strain rate, changing the temperature from RT to 300 °C, caused a dramatic decrease in strength and noticeable increase in ductility, as expected. More specifically, the tensile strength of a specimen deteriorated 85% but ductility recovered 350% by changing the temperature from RT to 300 °C at the low strain rate. In addition, the tensile strength of a specimen deteriorated 70% but ductility recovered 160% by changing the temperature from RT to 300 °C at the high strain rate. The observed effect of temperature on the mechanical response has very well discussed in the literature and corresponds well with our results [33–35]. Moreover, at the same temperature (RT), increasing strain rate by 5 order of magnitudes decreased the stress values at fracture and increased the ductility. Furthermore, at the same temperature (300 °C), increasing strain rate by 5 order of magnitudes increased the tensile strength and decreased the ductility. Consequently, both the positive strain rate sensitivity (PSRS) and negative strain rate sensitivity (NSRS) were observed at different temperatures. Specifically, when the material was deformed at the high temperature (300 °C) and faster rate, the diffusion velocity of

substitutional atoms and the rate of generation of forest dislocations also increased [36]. When the material was deformed at RT, the substitutional atoms (Table 1) stayed longer at the lattice site at lower strain rate and pinned the movement of dislocation by acting as barrier against dislocation motion and created additional contribution to the overall hardening (NSRS). However, at the high strain rate this pinning effect was not significant since both the generation rate of dislocations and diffusion velocity of substitutional atoms were higher compared to low strain rate case [37]. However, at high temperature, the substitutional atoms were activated and started their movement and could not pin the dislocations. That is why, no pinning effect was observed at the high temperature case and PSRS was observed. Specifically, much more dislocation got activated when the material was deformed at faster rate and forest hardening dominated the overall hardening response and stress levels at the same strain values increased by increasing strain rate. Our results correspond well with the literature [38–40]. The Gleeble test results were also used for the calculation of J-C material and damage model parameters (Table 9, 10).

4.4 Determination of J-C Material Parameters

J-C material model parameters were only determined for the material along the rolling direction since the J-C material model is designed for ductile materials and the material perpendicular to the rolling direction showed brittle behavior (Figure 4). For the determination of the J-C material model constants, basically three different experimental works were conducted. Firstly, in order to determine the flow curve of Al 7068-T651 in quasi-static condition, tensile test data of Gleeble 3800-GTC was used since the system has a high-speed servo valve system to have a high precision and quick response in desired strain rates.

The quasi-static tests are conducted at a strain rate of 10^{-3} s^{-1}. The obtained true strain vs. true stress data from the quasi-static tests are displayed in Figure 9. By processing these data and performing Ludwik fit to the flow curves, A, B and n values of J-C material model were determined (Figure 10), where ϵ is the true plastic strain and σ is the flow stress. The overall results of the three quasi-static tests are illustrated in Table 10 in order to provide the reasonable precision level of the experiments. There is one study, which lists the Johnson Cook material model coefficients of Al 7068 alloy, in the literature [41] but this study does not specify the heat treatment condition (temper code) of the alloy.

During SHPB tests, there different pressure values were used to provide 1800, 2500 and 5000 s^{-1} strain rates respectively. A sample of the incident and transmitted shock waves from the experimental studies are shown in the Figure 11. After having obtained the data from high strain rate tests, the flow stress values at the plastic strain of 0.050 (the offset stress value) were determined. In order to determine the offset stresses, a parallel line was constructed to the loading curves and the intersection point of this parallel line with the existing true strain vs. true stress curve was computed by means of a specifically created MatLab script. This methodology was explained schematically in Figure 12 for the 1800 s^{-1} strain rate case. This procedure was repeated in order to determine the offset stresses for each specific strain rate. The computed values are listed in Table 11. Then, the necessary curve fitting algorithms were employed in MatLab environment by means of which the strain rate sensitivity coefficient of J-C material models was determined as -0.08581, which is the coefficient of "C" in Eq. 2. Negative C parameter means that Al 7068-T651 exhibits negative strain rate (NSR) sensitivity.

And lastly, the thermal softening exponent "m" of J-C material model was computed by processing the quasi-static test (0.001 s^{-1}) at 300 °C. The 0.05 offset stress was computed

by the aforementioned methodology and the MatLab script. By implementing the curve-fitting operation in Matlab, the parameter "m" was determined as 4.2285. The obtained offset stress values of quasi-static 300 °C tests were listed in Table 12.

5. Conclusions

In this study, the effects of the rolling direction, STF, strain rate and temperature on the mechanical response of Al 7068-T651 alloy were investigated by uniaxial tensile tests, SHPB tests and Gleeble tests. Then, by utilizing the Levenberg-Marquardt optimization method, which was applied on an iterative code through Matlab, J-C damage model constants, D_1, D_2 and D_3, based on maximum and minimum equivalent strain values were also determined since these can be used for the simulation of different applications. In addition, D_4 and D_5 were calculated based on Gleeble test results and all the J-C material model parameters were determined using Gleeble and SHPB test results. From the work presented herein the following conclusions, related to mechanical response, can be drawn:

1) As the STF is increasing, both strength and ductility of the alloy also increase for the specimen along the rolling direction while the smooth specimen has the greatest strength at the same elastic strain values compared to other specimens. On the contrary, for specimens in perpendicular to rolling direction, as the STF increases, only ductility of the alloy increases.
2) Al 7068-T651 alloy has anisotropic mechanical properties and changing the direction from along the rolling to perpendicular to the rolling direction deteriorates the mechanical properties of the Al7068-T651 alloy. On the contrary, within the elastic range, Al 7068-T651 alloy perpendicular to the rolling direction has greater strength values at the same strain compared to materials along the rolling direction. Thus, specimen perpendicular to the rolling direction can be used over Al 7068-

T651 alloy along rolling direction in applications where high ductility is not required.

3) Even though as the stress triaxiality increases, the failure strain of the Al 7068-T651 along the rolling direction always decreases, it was observed that a critical notch radius might enhance the failure strain of the Al 7068-T651 alloy perpendicular to the rolling direction.

Overall, this study investigates for the first time the effects of rolling direction, temperature, strain rate and STF on the mechanical response of Al 7068-T651 alloy. In addition, D_1, D_2 and D_3 damage parameters were determined very precisely for different application areas for material both along the rolling direction and perpendicular to the rolling direction (Table 6, 7, 8). Moreover, the rest of the J-C damage parameters were determined accurately (Table 9). Furthermore, all the J-C material model parameters of Al 7068 were determined (Table 10). Consequently, this study opens a new venue for the selection and usage of the J-C damage and model parameters in Finite Element simulations.

Acknowledgments

B.Bal gratefully acknowledges the financial support provided by Aselsan A.Ş.

References

[1] Cole, G. S., and Sherman, A. M., 1995, "Light Weight Materials for Automotive Applications," Mater. Charact., **35**(1), pp. 3–9.

[2] Cobden, R., and Banbury, A., 1994, "Aluminium: Physical Properties, Characteristics and Alloys," Talal, **1994**(1994), p. 60.

[3] Davis, J. R., 2001, "Aluminum and Aluminum Alloys," Light Met. Alloy., p. 66.

[4] Davis, J. R., 1993, *ASM Specialty Handbook: Aluminum and Aluminum Alloys*.

[5] Dursun, T., and Soutis, C., 2014, "Recent Developments in Advanced Aircraft Aluminium Alloys," Mater. Des., **56**, pp. 862–871.

[6] Smiths Metal Centers, 2017, *7068 Aluminum Alloy Technical Datasheet*, United Kingdom.

[7] Minnicino, M., Gray, D., and Moy, P., 2009, *Aluminum Alloy 7068 Mechanical Characterization*, U.S.

[8] Zhang, Y., Outeiro, J. C., and Mabrouki, T., 2015, "On the Selection of Johnson-Cook Constitutive Model Parameters for Ti-6Al-4V Using Three Types of Numerical Models of Orthogonal Cutting," Procedia CIRP, **31**, pp. 112–117.

[9] Thepsonthi, T., and Özel, T., 2015, "3-D Finite Element Process Simulation of Micro-End Milling Ti-6Al-4V Titanium Alloy: Experimental Validations on Chip Flow and Tool Wear," J. Mater. Process. Technol., **221**, pp. 128–145.

[10] Onal, O., Bal, B., Canadinc, D., and Akdari, E., 2015, "Experimental and Numerical Evaluation of Thickness Reduction in Steel Plate Heat Exchangers," J. Eng. Mater. Technol. Trans. ASME, **137**(4), pp. 041001-041008.

[11] Onal, O., Bal, B., Toker, S. M., Mirzajanzadeh, M., Canadinc, D., and Maier, H. J., 2014, "Microstructure-Based Modeling of the Impact Response of a Biomedical Niobium–zirconium Alloy," J. Mater. Res., **29**(10), pp. 1123–1134.

[12] Valoppi, B., Bruschi, S., Ghiotti, A., and Shivpuri, R., 2017, "Johnson-Cook Based Criterion Incorporating Stress Triaxiality and Deviatoric Effect for Predicting Elevated

Temperature Ductility of Titanium Alloy Sheets," Int. J. Mech. Sci., **123**(January), pp. 94–105.

[13] Liu, R., Melkote, S., Pucha, R., Morehouse, J., Man, X., and Marusich, T., 2013, "An Enhanced Constitutive Material Model for Machining of Ti-6Al-4V Alloy," J. Mater. Process. Technol., **213**(12), pp. 2238–2246.

[14] Chen, G., Ren, C., Qin, X., and Li, J., 2015, "Temperature Dependent Work Hardening in Ti–6Al–4V Alloy over Large Temperature and Strain Rate Ranges: Experiments and Constitutive Modeling," Mater. Des., **83**, pp. 598–610.

[15] Brar, N. S., and Joshi, V. S., 2012, "Anisotropic Effects on Constitutive Model Parameters of Aluminum Alloys," AIP Conf. Proc., **1426**(1), pp. 72–75.

[16] Tan, J. Q., Zhan, M., Liu, S., Huang, T., Guo, J., and Yang, H., 2015, "A Modified Johnson-Cook Model for Tensile Flow Behaviors of 7050-T7451 Aluminum Alloy at High Strain Rates," Mater. Sci. Eng. A, **631**, pp. 214–219.

[17] Zhang, D. N., Shangguan, Q. Q., Xie, C. J., and Liu, F., 2015, "A Modified Johnson-Cook Model of Dynamic Tensile Behaviors for 7075-T6 Aluminum Alloy," J. Alloys Compd., **619**, pp. 186–194.

[18] Brar, N. S., Joshi, V. S., and Harris, B. W., 2009, "Constitutive Model Constants for Al7075-T651 and Al7075-T6," AIP Conf. Proc., **1195**(1), pp. 945–948.

[19] Moré, J. J., 1978, *The Levenberg-Marquardt Algorithm: Implementation and Theory.*, Springer, Berlin, Heidelberg.

[20] Gaidhane, V. H., Hote, Y. V., and Singh, V., 2012, "Nonrigid Image Registration Using Efficient Similarity Measure and Levenberg-Marquardt Optimization," Biomed.

Eng. Lett., **2**(2), pp. 118–123.

[21] Vening Meinesz, F. A., 1956, "Elasticity and Plasticity," Appl. Sci. Res. Sect. A, **6**(2–3), pp. 205–225.

[22] Bobbili, R., Paman, A., and Madhu, V., 2016, "High Strain Rate Tensile Behavior of Al-4.8Cu-1.2Mg Alloy," Mater. Sci. Eng. A, **651**, pp. 753–762.

[23] Algarni, M., Bai, Y., and Choi, Y., 2015, "A Study of Inconel 718 Dependency on Stress Triaxiality and Lode Angle in Plastic Deformation and Ductile Fracture," Eng. Fract. Mech., **147**, pp. 140–157.

[24] Keshavarz, A., Ghajar, R., and Mirone, G., 2014, "A New Experimental Failure Model Based on Triaxiality Factor and Lode Angle for X-100 Pipeline Steel," Int. J. Mech. Sci., **80**, pp. 175–182.

[25] Bridgman, P. W., 1952, *Studies in Large Flow and Fracture*, New York: McGraw-Hill.

[26] Bao, Y., 2003, "Prediction of Ductile Crack Formation in Uncracked Bodies," PhD Thesis, p. 252.

[27] Bao, Y., and Wierzbicki, T., 2004, "On Fracture Locus in the Equivalent Strain and Stress Triaxiality Space," Int. J. Mech. Sci., **46**(1), pp. 81–98.

[28] Bai, Y., Teng, X., and Wierzbicki, T., 2009, "On the Application of Stress Triaxiality Formula for Plane Strain Fracture Testing," J. Eng. Mater. Technol., **131**(2), pp. 1–10.

[29] Neimitz, A., Galkiewicz, J., Lipiec, S., and Dzioba, I., 2018, "Estimation of the Onset of Crack Growth in Ductile Materials," Materials (Basel)., **11**(10), p. 2026.

[30] Senthil, K., Iqbal, M. A., Chandel, P. S., and Gupta, N. ., 2017, "Study of the Constitutive Behavior of 7075-T651 Aluminum Alloy," Int. J. Impact Eng., **000**.

[31] Mirzajanzadeh, M., and Canadinc, D., 2016, "A Microstructure-Sensitive Model for Simulating the Impact Response of an High-Manganese Austenitic Steel," J. Eng. Mater. Technol., **138**(March 2015), pp. 1–14.

[32] Majzoobi, G. H., and Dehgolan, F. R., 2011, "Determination of the Constants of Damage Models," Procedia Eng., **10**, pp. 764–773.

[33] Magnus Hörnqvista and Birger Karlssonb, 2006, "Temperature and Strain Rate Effects on the Dynamic Strain Ageing of Aluminium Alloy AA7030," Mater. Sci. Forum, **519–521**, pp. 883–888.

[34] Li, D., and Ghosh, A., 2003, "Tensile Deformation Behavior of Aluminum Alloys at Warm Forming Temperatures," Mater. Sci. Eng. A, **352**(1–2), pp. 279–286.

[35] Lee, W. S., Sue, W. C., Lin, C. F., and Wu, C. J., 2000, "Strain Rate and Temperature Dependence of the Dynamic Impact Properties of 7075 Aluminum Alloy," J. Mater. Process. Technol., **100**(1), pp. 116–122.

[36] Onal, O., Ozmenci, C., and Canadinc, D., 2014, "Multi-Scale Modeling of the Impact Response of a Strain-Rate Sensitive High-Manganese Austenitic Steel," Front. Mater., **1**(September), pp. 1–12.

[37] Bal, B., Gumus, B., and Canadinc, D., 2016, "Incorporation of Dynamic Strain Aging into a Viscoplastic Self-Consistent Model for Predicting the Negative Strain Rate Sensitivity of Hadfield Steel," J. Eng. Mater. Technol. Trans. ASME, **138**(3), pp. 1–8.

[38] Canadinc, D., Efstathiou, C., and Sehitoglu, H., 2008, "On the Negative Strain Rate Sensitivity of Hadfield Steel," Scr. Mater., **59**(10), pp. 1103–1106.

[39] Chmelík, F., Klose, F. B., Dierke, H., Šachl, J., Neuhäuser, H., and Lukáč, P., 2007,

"Investigating the Portevin-Le ChâTelier Effect in Strain Rate and Stress Rate Controlled Tests by the Acoustic Emission and Laser Extensometry Techniques," Mater. Sci. Eng. A, **462**, pp. 53–60.

[40] Chen, L., Kim, H.-S., Kim, S.-K., and De Cooman, B. C., 2007, "Localized Deformation Due to Portevin–LeChatelier Effect in 18Mn–0.6C TWIP Austenitic Steel," ISIJ Int., **47**(12), pp. 1804–1812.

[41] Collinson, M., 2014, "On The Characterisation Of Shock-Induced Sliding Along Multi-Material Interfaces."

Table 1. Chemical composition of the studied material (in wt. %).

Fe	Cu	Mn	Mg	Cr	Zn	Zr	Si	Al
0.15	3.79	0.1	3.75	0.05	11.7	0.05	0.13	Balance

Table 2: Stress triaxiality factors and gauge lengths for each configuration.

Notch Radius (mm)	Gauge Length (mm)	σ^*
Smooth	5	0.33
R0.4	0.74	1.39
R0.8	1.52	0.99
R2	3.46	0.65

Journal of Engineering Materials and Technology. Received December 26, 2018;
Accepted manuscript posted February 06, 2019. doi:10.1115/1.4042870

Table 3: Initial and fracture cross-section areas of the tensile tested specimens.

Rolling Direction	Notch Radius (mm)	Initial Area (mm^2)	Final area (mm^2)
Along The Rolling Direction	Smooth	7.06	5.78
	0.4	7.06	6.44
	0.8	7.06	6.07
	2	7.06	6.00
Perpendicular To The Rolling Direction	Smooth	7.06	6.81
	0.4	7.06	6.97
	0.8	7.06	7.02
	2	7.06	6.60

Table 4: Initial and fracture cross-section areas of the Gleeble test specimens.

Temperature	Strain Rate (s^{-1})	Initial Area (mm^2)	Final area (mm^2)
RT	10^2	28,27	22,54
RT	10^{-3}	28,27	23,15
300 °C	10^2	28,27	11,25
300 °C	10^{-3}	28,27	6,09

Table 5: Yield strength, tensile strength and elongation values of smooth and notch specimens.

Rolling Direction	Notch Radius	Yield Strength	Tensile Strength	Engineering Strain at fracture	True Strain at fracture

Journal of Engineering Materials and Technology. Received December 26, 2018;
Accepted manuscript posted February 06, 2019. doi:10.1115/1.4042870

	(mm)	(MPa)	(MPa)	(mm/mm)	(mm/mm)
Along The Rolling Direction	Smooth (0)	708	819	0.10021	0.0955
	0.4	837	1510	0.49323	0.40094
	0.8	812	1170	0.25052	0.22356
	2	763	947	0.11855	0.11204
Perpendicular to The Rolling Direction	Smooth (0)	503	642	0.05579	0.05429
	0.4	-	531	0.19076	0.17459
	0.8	-	671	0.12018	0.11349
	2	-	638	0.05179	0.05049

Table 6: Johnson-Cook damage model constants for Al7068-T651 alloy with maximum equivalent plastic strain values.

J-C Damage Constant	Rolling Direction	Perpendicular to the rolling direction
D1	0.1211	0.0269
D2	0.4535	0.0374
D3	-2.6445	-4.1040

Table 7: Johnson-Cook damage model constants for Al7068-T651 alloy with average equivalent plastic strain values.

J-C Damage Constant	Rolling Direction	Perpendicular to the rolling direction
D1	0.1009	0.0130
D2	0.1214	0.0359
D3	-0.9150	-3.1844

Table 8: Johnson-Cook damage model constants for Al7068-T651 alloy with minimum equivalent plastic strain values.

J-C Damage Constant	Rolling Direction	Perpendicular to the rolling direction

Journal of Engineering Materials and Technology. Received December 26, 2018;
Accepted manuscript posted February 06, 2019. doi:10.1115/1.4042870

D1	0.0678	0.0066
D2	0.0604	0.0304
D3	-0.0251	-3.1844

Table 9: Johnson-Cook damage model constants for Al7068-T651 alloy

J-C Damage Constant	Rolling Direction
D4	-0.16789
D5	0.877675

Table 10: J-C material model constants (A, B, C, n and m) for Al7068-T651 alloy

	A	B	C	n	m
Sample-1	841.500	454.100	-0.08581	0.548	4.2285
Sample-2	825.500	495.600	-0.08581	0.573	4.2285
Sample-3	840.500	471.300	-0.08581	0.562	4.2285
Average	835.833	473.667	-0.08581	0.561	4.2285
Standard Deviation	7.318	17.025	0	0.010	0
Standard Deviation (%)	0.009	0.036	0	0.018	0

Table 11: Offset stresses at high strain rate tests for Al7068-T651 alloy

		1800 s^{-1}	2800 s^{-1}	5000 s^{-1}
0.05 Offset Stresses	**Sample-1**	821.79	828.50	828.82
	Sample-2	827.36	827.36	823.44
	Sample-3	825.10	823.96	825.24
	Average	824.75	826.61	825.83
	Standard	0.28%	0.23%	0.27%

Journal of Engineering Materials and Technology. Received December 26, 2018;
Accepted manuscript posted February 06, 2019. doi:10.1115/1.4042870

	Deviation (%)	

Table 12: Offset stresses at high temperature tests for Al7068-T651 alloy

		$0.001\ s^{-1}$-300 °C
0.05 Offset Stresses	**Sample-1**	110.99
	Sample-2	116.08
	Sample-3	115.24
	Average	114.10
	Standard Deviation (%)	1.95%

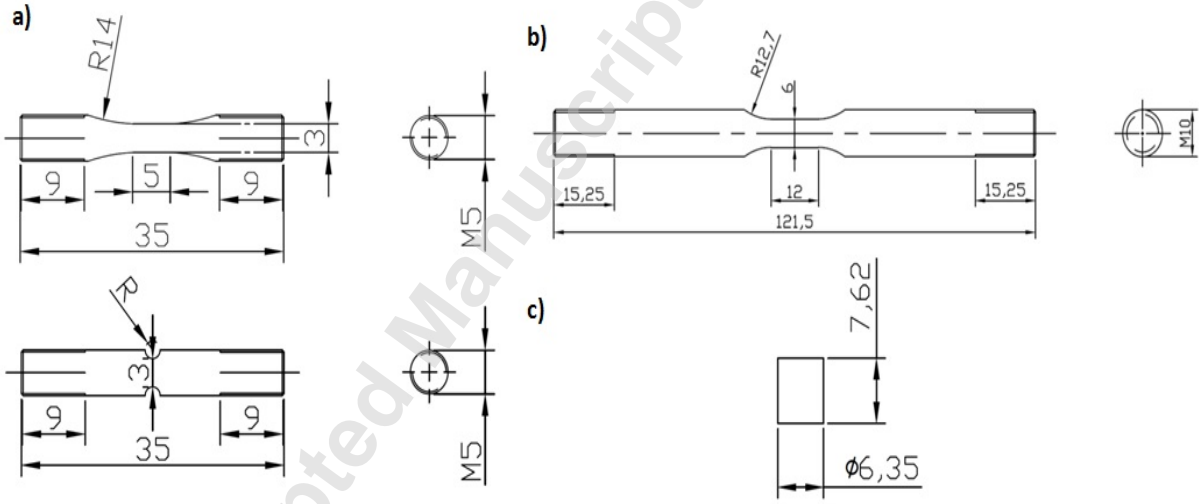

Figure 1. **a):** Specimen geometries of smooth specimen and notched specimen for tensile tests **b):** Specimen geometry for Gleeble tests **c):** Specimen geometry for SHPB tests (unit: mm).

Journal of Engineering Materials and Technology. Received December 26, 2018;
Accepted manuscript posted February 06, 2019. doi:10.1115/1.4042870

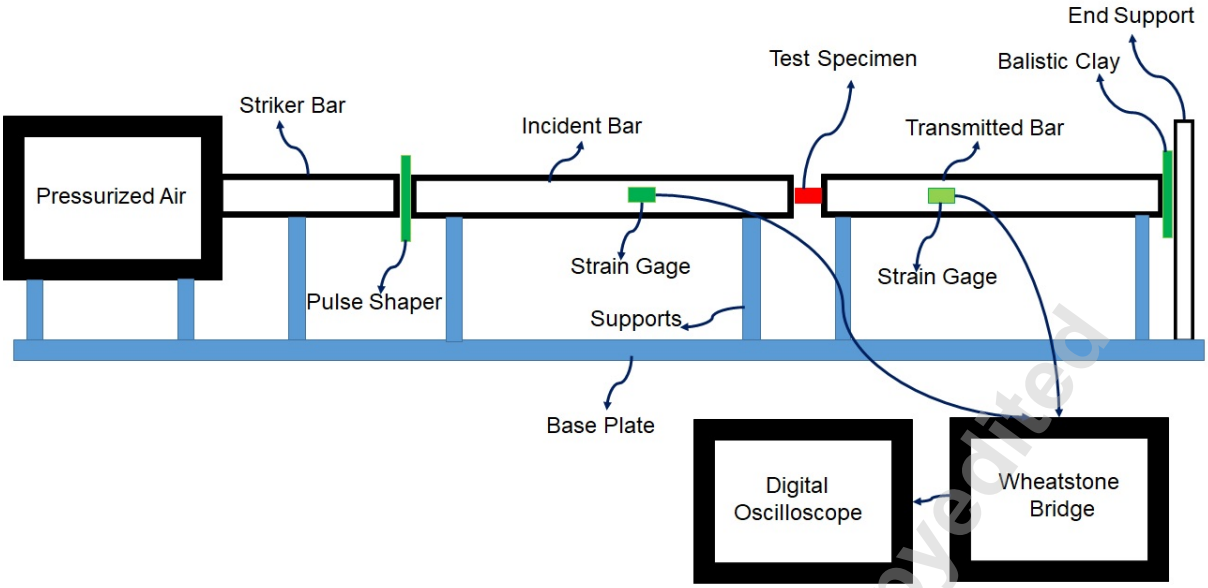

Figure 2: Schematic representation of the custom-made Split Hopkinson Pressure Bar setup.

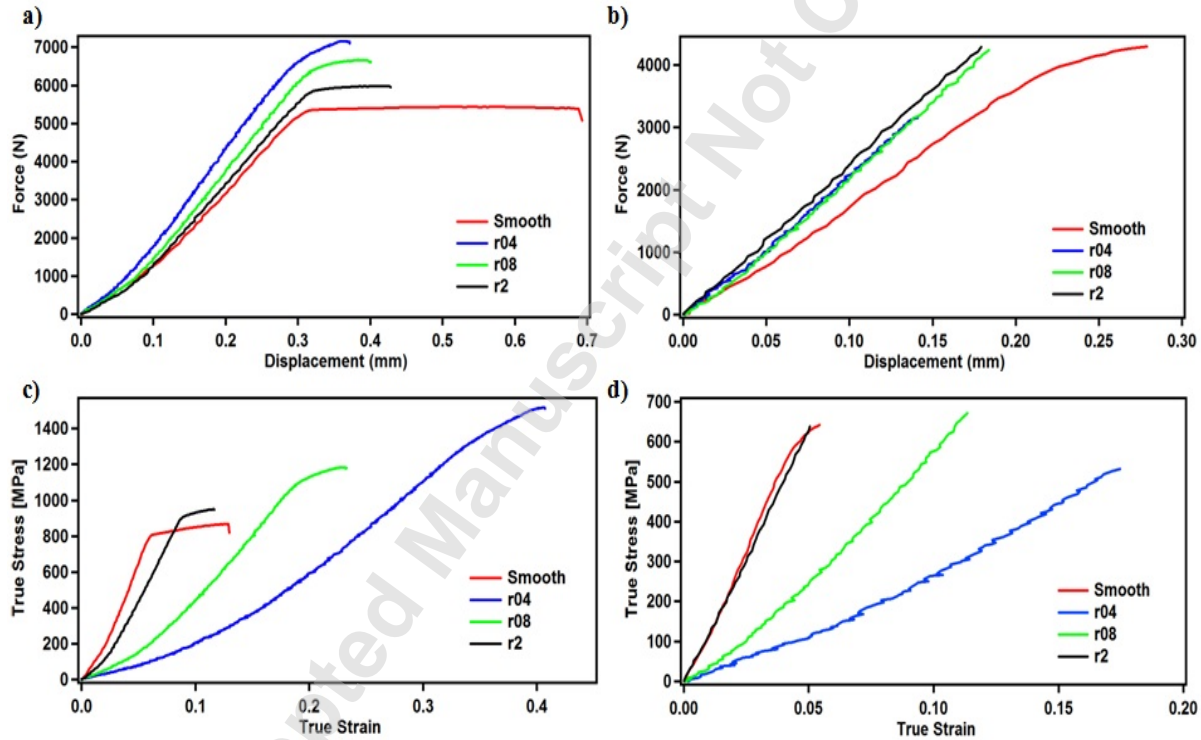

Figure 3: Force versus displacement graphs of Al 7068-T651 alloy a) along the rolling direction b) perpendicular to the rolling direction and true stress – true strain behavior of Al 7068-T651 alloy c) along the rolling direction d) perpendicular to the rolling direction.

Journal of Engineering Materials and Technology. Received December 26, 2018;
Accepted manuscript posted February 06, 2019. doi:10.1115/1.4042870

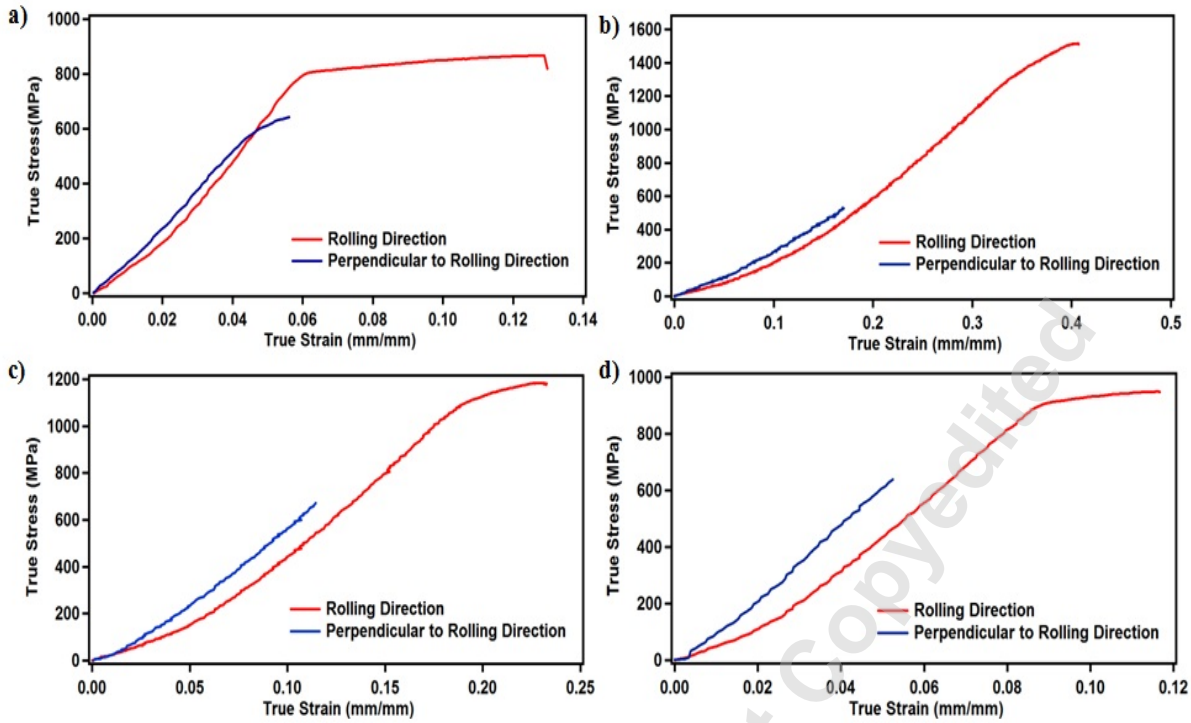

Figure 4: Comparison of the tensile behavior between the rolling direction and perpendicular to the rolling direction a) smooth specimens b) R0.4 c) R0.8 d) R2.

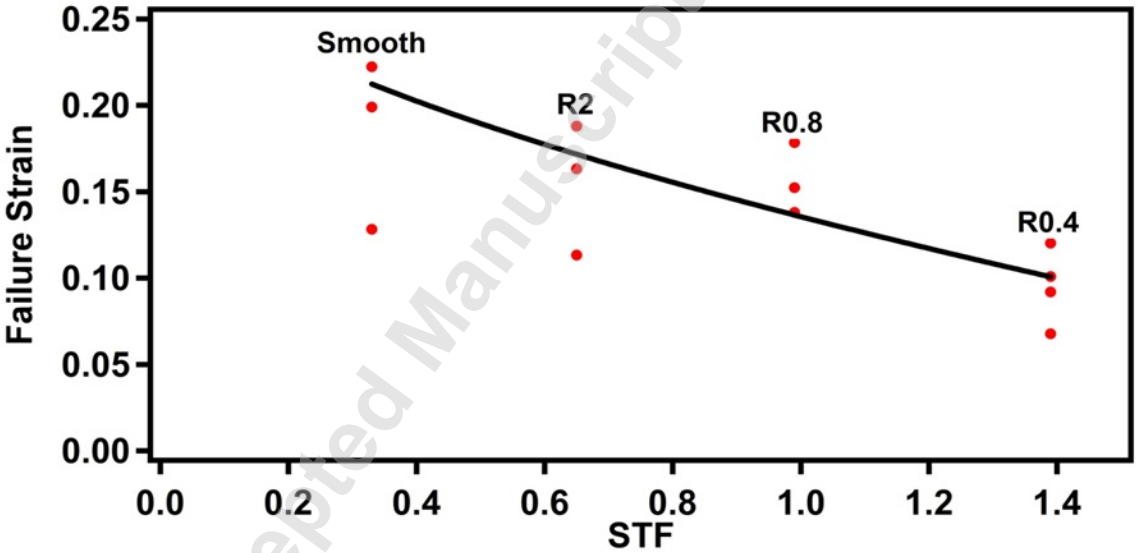

Figure 5: Equivalent plastic strain to fracture vs. STF for the specimen in the rolling direction.

Journal of Engineering Materials and Technology. Received December 26, 2018;
Accepted manuscript posted February 06, 2019. doi:10.1115/1.4042870

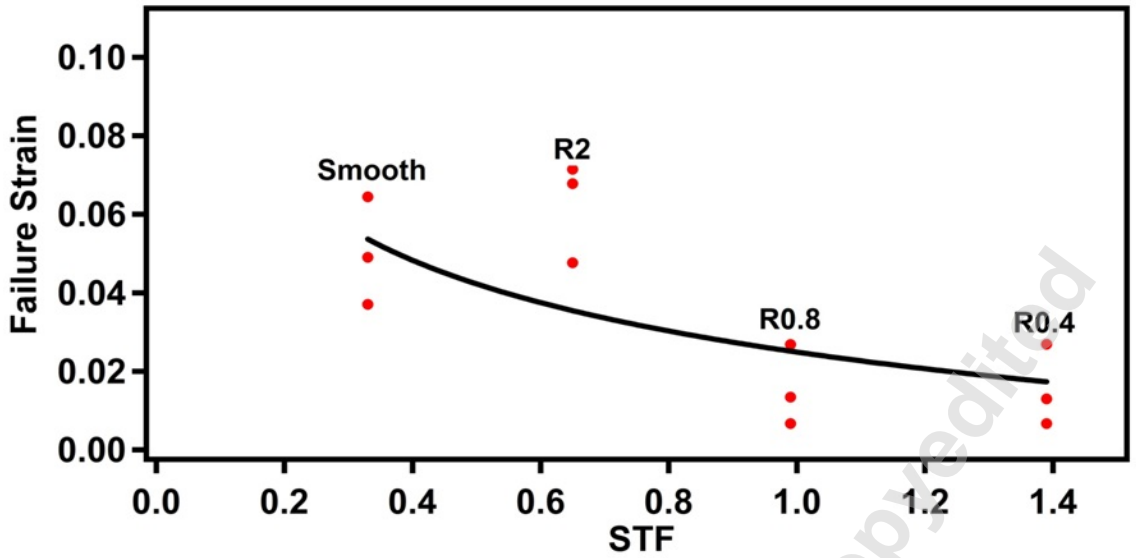

Figure 6: Equivalent plastic strain to fracture vs. STF for the specimen perpendicular to the rolling direction.

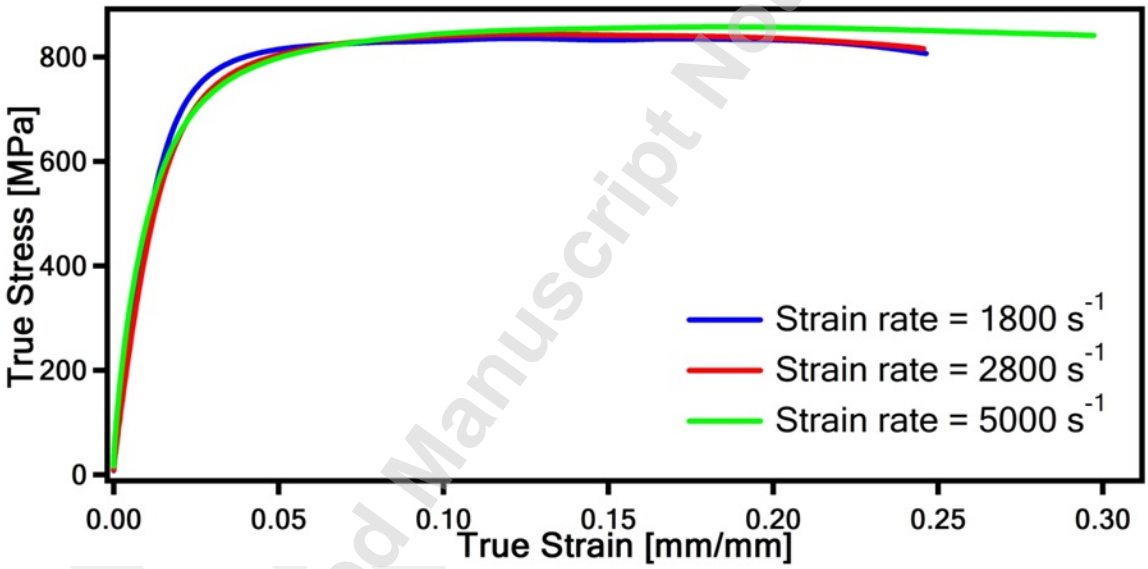

Figure 7: True stress vs true strain response of Al 7068-T651 under SHPB loading.

Journal of Engineering Materials and Technology. Received December 26, 2018;
Accepted manuscript posted February 06, 2019. doi:10.1115/1.4042870

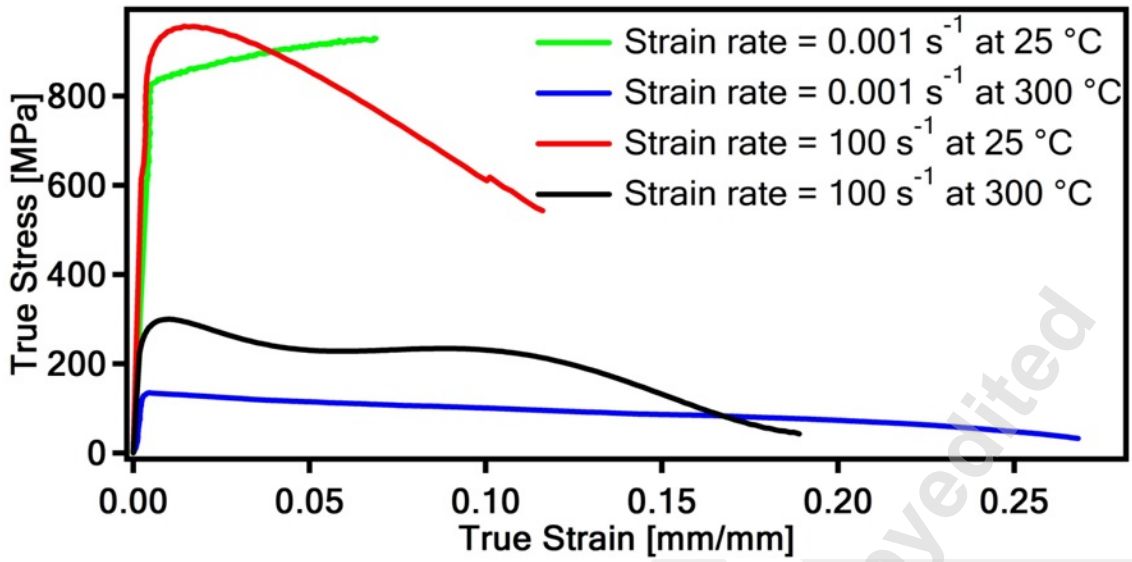

Figure 8: True stress vs true strain response of Al 7068-T651 from Gleeble tests.

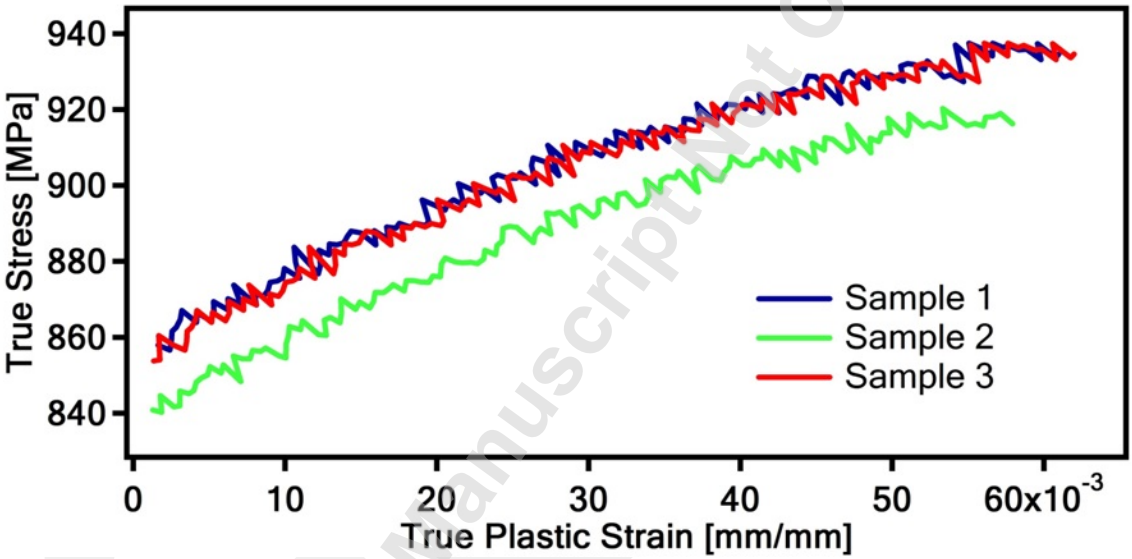

Figure 9: True stress vs. true strain data of quasi-static tests.

Journal of Engineering Materials and Technology. Received December 26, 2018;
Accepted manuscript posted February 06, 2019. doi:10.1115/1.4042870

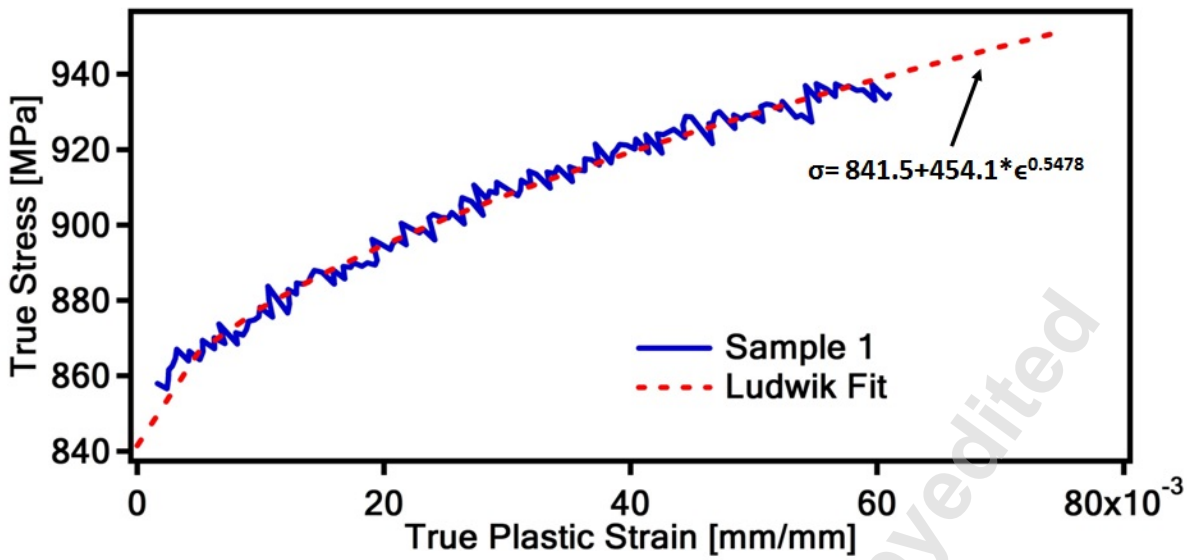

Figure 10: Determination of A, B and n parameters of J-C Material Model for Al 7068-T651

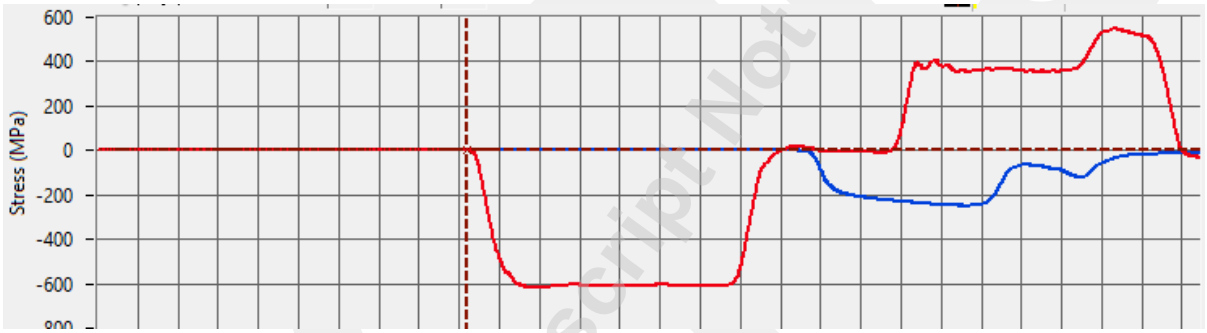

Figure 11: A representative shockwave generated by the SHPB test system

Journal of Engineering Materials and Technology. Received December 26, 2018;
Accepted manuscript posted February 06, 2019. doi:10.1115/1.4042870

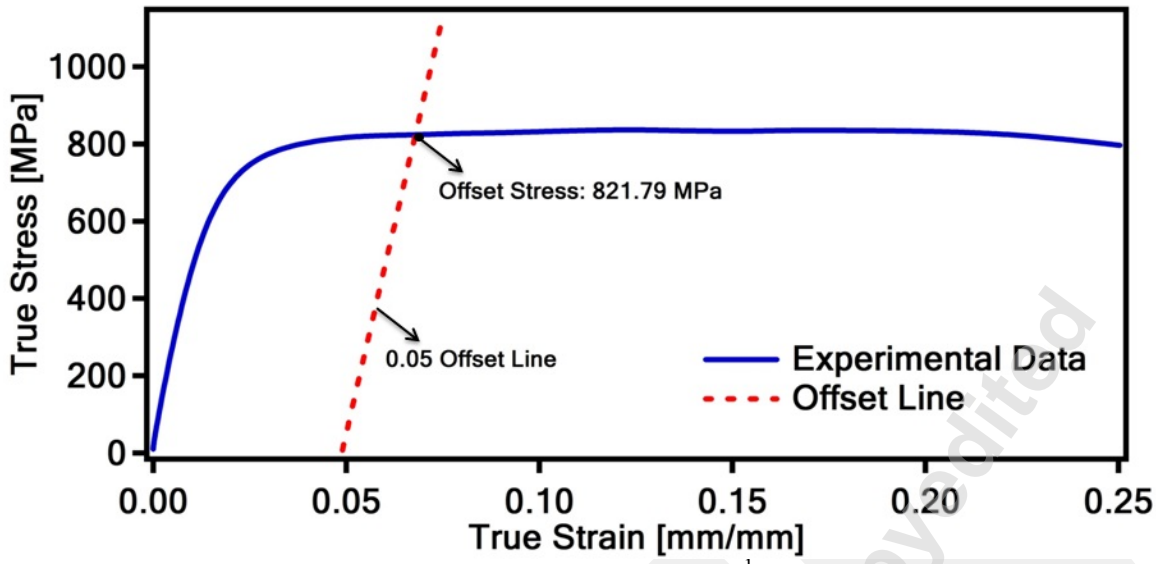

Figure 12: Determination of the offset stress at the 1800 s^{-1} case.